

---

# Improvement of Algan Homoepitaxial Tunnel Junction Deep-UV Light-Emitting Diodes by Controlling the Growth of N-Type Algan and Polycrystalline Mgzno/Al Electrodes

---

[Kengo Nagata](#)<sup>\*</sup>, Taichi Matsubara, Yoshiki Saito, Keita Kataoka, Tetsuo Narita, Kayo Horibuchi, Maki Kushimoto, Shigekazu Tomai, [Satoshi Katsumata](#), Yoshio Honda, [Tetsuya Takeuchi](#), [Hiroshi Amano](#)

Posted Date: 17 February 2023

doi: 10.20944/preprints202302.0249.v2

Keywords: AlGaIn; tunnel junction; light-emitting diode; deep-ultraviolet; MgZnO



Preprints.org is a free multidiscipline platform providing preprint service that is dedicated to making early versions of research outputs permanently available and citable. Preprints posted at Preprints.org appear in Web of Science, Crossref, Google Scholar, Scilit, Europe PMC.

Copyright: This is an open access article distributed under the Creative Commons Attribution License which permits unrestricted use, distribution, and reproduction in any medium, provided the original work is properly cited.

Review

# Improvement of AlGa<sub>N</sub> Homoepitaxial Tunnel Junction Deep-UV Light-Emitting Diodes by Controlling the Growth of n-Type AlGa<sub>N</sub> and Polycrystalline MgZnO/Al Electrodes

Kengo Nagata <sup>1,\*</sup>, Taichi Matsubara <sup>2</sup>, Yoshiki Saito <sup>1</sup>, Keita Kataoka <sup>3</sup>, Tetsuo Narita <sup>3</sup>, Kayo Horibuchi <sup>3</sup>, Maki Kushimoto <sup>2</sup>, Shigekazu Tomai <sup>4</sup>, Satoshi Katsumata <sup>4</sup>, Yoshio Honda <sup>5</sup>, Tetsuya Takeuchi <sup>6</sup> and Hiroshi Amano <sup>5</sup>

<sup>1</sup> Toyoda Gosei Co., Ltd., 710 Shimomiyakeoriguchi, Heiwa-cho, Inazawa, Aichi 290-1312, Japan; kengo.nagata@toyoda-gosei.co.jp; yoshiki.saito@toyoda-gosei.co.jp

<sup>2</sup> Graduate School of Engineering, Nagoya University, Furo-cho, Chikusa-ku, Nagoya, Aichi 464-8603, Japan; matsubara.taichi@i.mbox.nagoya-u.ne.jp; kushimoto@nuee.nagoya-u.ac.jp

<sup>3</sup> Toyota Central R&D Labs. Inc., Nagakute, Aichi 480-1192, Japan; e1354@mosk.tytlabs.co.jp; tetsuo-narita@mosk.tytlabs.co.jp; e4721@mosk.tytlabs.co.jp

<sup>4</sup> Advanced Technology Research Laboratories, Idemitsu Kosan Co., Ltd., 1280 Kamiizumi, Sodegaura, Chiba 299-0205, Japan; shigekazu.tomai.6560@idemitsu.com; satoshi.katsumata.6820@idemitsu.com

<sup>5</sup> Center for Integrated Research of Future Electronics, Institute of Materials and Systems for Sustainability, Nagoya University, Furo-cho, Chikusa-ku, Nagoya, Aichi 464-8601, Japan; honda@nagoya-u.jp; amano@nuee.nagoya-u.ac.jp

<sup>6</sup> Faculty of Science and Technology, Meijo University, 1-501 Shiogamaguchi, Tenpaku-ku, Aichi 468-8502, Japan; take@meijo-u.ac.jp

\* Correspondence: kengo.nagata@toyoda-gosei.co.jp

**Abstract:** Deep-ultraviolet (UV) light-emitting diodes (LEDs) based on AlGa<sub>N</sub> crystals have low light-emission efficiency; therefore, there is a need to improve this light-emission efficiency for a wide range of applications such as water and air sterilizations. UV-light-transparent device structures are considered one of the many solutions toward increasing light output power. To this end, the present study focused on developing a transparent AlGa<sub>N</sub>-based tunnel junction (TJ) as the anode of a deep-UV LED. Deep-UV LEDs composed of n<sup>+</sup>/p<sup>+</sup>-type AlGa<sub>N</sub> TJs were fabricated under the growth condition that reduced the carrier compensation in the n<sup>+</sup>-type AlGa<sub>N</sub> layers. The operating voltage was 10.8 V under the direct current (DC) operation of 63 A/cm<sup>2</sup>. In addition, magnesium zinc oxide (MgZnO)/Al reflective electrodes were fabricated to enhance the output power of the AlGa<sub>N</sub> homoepitaxial TJ LED. The output power was 57.3 mW under a DC operation of 63 A/cm<sup>2</sup>, and it was 1.7 times higher than that realized using the conventional Ti/Al electrodes. The combination of the AlGa<sub>N</sub>-based TJ and MgZnO/Al reflective contact allows further improvement of the light output power. This study confirms that the AlGa<sub>N</sub> TJ is a promising UV-transmittance structure that can obtain a high light-extraction efficiency.

**Keywords:** AlGa<sub>N</sub>, tunnel junction, light-emitting diode, deep-ultraviolet, MgZnO

## 1. Introduction

Aluminum gallium nitride (AlGa<sub>N</sub>)-based light-emitting diodes (LEDs) emit deep-ultraviolet (UV) light and are utilized in several applications at different wavelengths such as in curing, sensing, and water and air sterilizations. These LEDs are considered replacements for the mercury lamps used in water and air sterilizations [1–3]. Deep-UV light with an emission wavelength below 290 nm can rapidly inactivate the deoxyribonucleic acid of virus and bacteria [4,5]; however, the light-emission efficiency (LEE) of deep-UV LEDs is considerably lower than that of low-pressure mercury lamps. The wall-plug efficiency of mass-produced deep-UV LEDs is a maximum of 10% because of the UV

light absorption of the p-type gallium nitride (GaN) contact layer [6–8]. A p-type GaN contact layer is used in mass-produced deep-UV LEDs because a higher Al composition p-type AlGaN can lead to a higher ionization energy of magnesium (Mg) acceptors and a lower hole concentration [9–14]. Deep-UV LEDs with p-type AlGaN contact layers exhibited external quantum efficiencies (EQEs) of 10%–20% when rhodium (Rh) electrodes, patterned sapphire substrates, and resin encapsulations were used [15,16]. However, the wall-plug efficiencies (WPEs) of these deep-UV LEDs were not still high because of the increased contact resistivities between the electrodes and p-type AlGaN contact layers. By contrast, suitable electrode materials such as vanadium are available for n-type AlGaN-based cathode contacts [17–19].

One solution to this problem is forming a tunnel junction (TJ) for the anode contact of a deep-UV LED, because an n-type electrode with a low contact resistance is available. Table 1 lists previously reported LEDs having TJ-based anode contacts [20–31]. Some issues are faced in realizing a TJ-LED with a high-Al composition. The first issue is the difficulty of dehydrogenation from the buried p-type III-nitride layers. When using metalorganic vapor phase epitaxy (MOVPE) growth that is suitable for manufacturing LEDs, Mg acceptors are passivated by the hydrogen atoms in the growth ambient, resulting in a high resistivity [32,33]. Then, hydrogen atoms mostly locate at interstitial sites in III-nitrides [14]. An interstitial hydrogen atom is predicted to be charged positively and to be mobile in the p-type layer, whereas it would have a negative charge and be less mobile in the n-type layer [34]. Dehydrogenation from the p-type GaN layer buried under the n-type GaN has been reported to be difficult [35]. To avoid this problem, TJ layers were grown in the hydrogen-free ambient by methods such as plasma-enhanced molecular beam epitaxy (PAMBE) [20,22,26–30] as it results in a lower differential specific resistivity ( $R_s$ ) compared with that in the case of conventional MOVPE growth [21,23–25,31]. Recently, Akasaka et al. demonstrated the low resistivity of the n<sup>+</sup>-type GaN/p<sup>+</sup>-type GaN TJ using MOVPE growth by optimizing the doping profile and growth condition [25]; this should contribute toward the manufacture of GaN-based TJ contacts.

The second issue is the fact that the formation of highly-conductive TJs is more challenging for AlGaN-based TJs than for GaN-based ones, as seen from Table 1. This is caused by the increased tunneling barrier when the Al content increases. Deep-UV LEDs having AlGaN-TJ anode contacts reportedly enhanced the LEE; specifically, the LEE was high, and the operation voltages remained high in the range of 13–50 V [30,31]. To enhance the conductivity of the anode contact, Zhang et al. reported TJ double-heterostructures comprising n<sup>+</sup>-AlGaN/(Ga)InN/p<sup>+</sup>-AlGaN, in which the polarization charges reduced the TJ thickness [26–28]. The integration with the polarization doping technique using a graded AlGaN TJ layer was also effective in attracting high density free holes, resulting in enhanced tunneling probability [26].

A simpler way to increase the tunneling probability is to increase the doping concentration of tunneling homojunction layers. However, the resistivities of high-Al-content n-type AlGaN layers with high Si-doping concentrations ( $>6 \times 10^{19} \text{ cm}^{-3}$ ) were found to be extremely high because of the self-compensation caused by cation–vacancy–silicon ( $V_{\text{III}}\text{-nSi}$ ) complexes [32–41]. Further, carbon atoms were reported to cause carrier compensation by substituting nitrogen sites ( $C_N$ ) and to reduce the conductivities of n-type GaN layers [42–45]. The similar carrier compensation via  $C_N$  was predicted for an AlN-based material [46]. The growth condition of the high-Si-doped n<sup>+</sup>-type AlGaN needs to be controlled for suppressing the carrier compensation defects and reducing the operating voltage of AlGaN TJ LEDs.

The design of the electrode structure for light extraction from the backside is also important for deep-UV LEDs [47,48]. The output power can be enhanced using a high reflective electrode on the top. In visible-light LEDs, highly reflective metals combined with UV-transparent and conductive oxide electrodes are widely used to improve the LEE [49,50]. Examples of such oxide elements include indium tin oxide [51,52], indium-doped zinc oxide [53–55], aluminum-doped zinc oxide [56–58], and gallium-doped zinc oxide [59,60]. High reflective electrodes can be produced by stacking Al metals or a distributed Bragg reflector on these oxide electrodes, resulting in a reflectivity of 80%–90% [49,50]. Visible-light LEDs with high LEE can also be obtained by applying these reflective structures. However, these oxide materials have an absorption deep-UV region owing to bandgap

energies of 3.34–4.3 eV. We focus on high-Al composition AlGaIn TJ LEDs and magnesium zinc oxide (MgZnO)/Al reflective electrode. An MgZnO is suitable for suppressing the UV light absorption, and its bandgap can be controlled in the range of 3.34 to 7.8 eV by controlling the Mg/Zn composition [61,62]. A previous study reported that the MgZnO formed by the sputtering had two crystalline structures after recrystallization by annealing; both structures exhibited high transmittance in the UV range and n-type conductivity [63]. The conductivity was improved because of the mixture of both wurtzite structure MgZnO and rock salt structure or the oxygen vacancies in wurtzite structure MgZnO. The resistivity and transmittance of MgZnO were  $1.1 \times 10^{-1} \Omega\text{cm}$  and 20%, respectively [63]. There have been reports of improving the LEE of UV-A LEDs using MgZnO [64,65], but there have been no reports of UV-C LEDs.

In this study, we review the key challenges faced in deep-UV LEDs with AlGaIn-based TJ anode contacts. The growth conditions of the n<sup>+</sup>-type AlGaIn of TJ are controlled such that carbon incorporation can be suppressed at high Si doping to reduce the operating voltage of the AlGaIn TJ LED. Further, we demonstrate that MgZnO/Al reflective electrodes can fully exploit the transparent structure of TJs, which results in enhancing the LEE of deep-UV LEDs.

**Table 1. Summary of the III-nitride TJs reported previously, where  $V_F$  is a forward operation voltage and  $R_s$  is a differential specific resistivity.**

| Ref. | TJ structure   | Growth method              | $V_F$ (V)                   | $R_s$ ( $\Omega\text{cm}^2$ ) |
|------|--|----------------------------|-----------------------------|-------------------------------|
| [20] | n <sup>+</sup> -GaIn/GaN/p <sup>+</sup> -GaIn  | PAMBE                      | 3.05 @100 A/cm <sup>2</sup> | $1.2 \times 10^{-4}$          |
| [21] | n <sup>+</sup> -GaIn/p <sup>+</sup> -Ga <sub>0.6</sub> In <sub>0.4</sub> N   | MOVPE                      |                             | $4.0 \times 10^{-3}$          |
| [22] | n <sup>+</sup> -GaIn/p <sup>+</sup> -GaIn  | MOVPE+NH <sub>3</sub> -MBE | ~5 @100 A/cm <sup>2</sup>   | $2.3 \times 10^{-4}$          |
| [23] | n <sup>+</sup> -GaIn/p <sup>+</sup> -GaIn  | MOVPE                      | 5.92 @2 A/cm <sup>2</sup>   | $2.6 \times 10^{-1}$          |
| [24] | n <sup>+</sup> -GaIn/p <sup>+</sup> -GaIn $\mu$ -LED   | MOVPE                      | ~4 @20 A/cm <sup>2</sup>    | $2.5 \times 10^{-5}$          |
| [25] | n <sup>+</sup> -GaIn/p <sup>+</sup> -GaIn  | MOVPE                      | ~4 @100 A/cm <sup>2</sup>   | $2.4 \times 10^{-4}$          |
| [26] | n <sup>+</sup> -Al <sub>0.55</sub> Ga <sub>0.45</sub> N/ Ga <sub>0.8</sub> In <sub>0.2</sub> N<br>/p <sup>+</sup> -Al <sub>0.55</sub> Ga <sub>0.45</sub> N | PAMBE                      | 6.8 @10 A/cm <sup>2</sup>   | $1.5 \times 10^{-3}$          |
| [27] | n <sup>+</sup> -AlGaIn/ Ga <sub>0.8</sub> In <sub>0.2</sub> N<br>/graded p-AlGaIn  | PAMBE                      | 10.2 @10 A/cm <sup>2</sup>  | N/A                           |
| [28] | graded n <sup>+</sup> -AlGaIn<br>/ Ga <sub>0.8</sub> In <sub>0.2</sub> N/p <sup>+</sup> -Al <sub>0.65</sub> Ga <sub>0.35</sub> N                           | PAMBE                      | 10.5 @20 A/cm <sup>2</sup>  | $1.9 \times 10^{-3}$          |
| [29] | n <sup>+</sup> -Al <sub>0.65</sub> Ga <sub>0.35</sub> N/GaN<br>/p <sup>+</sup> -Al <sub>0.65</sub> Ga <sub>0.35</sub> N                                    | PAMBE                      | ~10 @100 A/cm <sup>2</sup>  | N/A                           |
| [30] | n <sup>+</sup> -Al <sub>0.5</sub> Ga <sub>0.5</sub> N/GaN<br>/p <sup>+</sup> -Al <sub>0.5</sub> Ga <sub>0.5</sub> N  | MOVPE+NH <sub>3</sub> -MBE | ~9 @100 A/cm <sup>2</sup>   | $1.2 \times 10^{-3}$          |
| [30] | n <sup>+</sup> -Al <sub>0.5</sub> Ga <sub>0.5</sub> N/p <sup>+</sup> -Al <sub>0.5</sub> Ga <sub>0.5</sub> N  | MOVPE+NH <sub>3</sub> -MBE | ~11 @100 A/cm <sup>2</sup>  | $1.7 \times 10^{-3}$          |
| [31] | n <sup>+</sup> -Al <sub>0.65</sub> Ga <sub>0.35</sub> N/n <sup>+</sup> -GaIn<br>/p <sup>+</sup> -Al <sub>0.65</sub> Ga <sub>0.35</sub> N                   | MOVPE                      | ~20                         | $(4-6) \times 10^{-3}$        |
| [31] | n <sup>+</sup> -Al <sub>0.65</sub> Ga <sub>0.35</sub> N<br>/p <sup>+</sup> -Al <sub>0.65</sub> Ga <sub>0.35</sub> N  | MOVPE                      | ~50                         | N/A                           |

## 2. Materials and Methods

Deep-UV LEDs were grown using a metalorganic vapor phase epitaxy on c-plane sapphire substrates with a miscut angle of  $0.35^\circ$  toward the sapphire [11 $\bar{2}$ 0] direction. Trimethylaluminum, trimethylgallium, triethylgallium, Bis(cyclopentadienyl)magnesium, monosilane gas, and ammonia gases were used as Al, Ga, Mg, Si, and N sources under hydrogen gas, respectively. The sapphire substrates were thermally cleaned in the H<sub>2</sub> ambient, and then, a 3- $\mu\text{m}$ -thick AlN was grown using a two-step growth technique [66]. Threading dislocation densities of screw and edge dislocations including mixed components in the AlN underlayer were estimated using an X-ray rocking curve at  $9 \times 10^7 \text{ cm}^{-2}$  and  $1 \times 10^9 \text{ cm}^{-2}$ , respectively [67]. The 1.3- $\mu\text{m}$ -thick n-type Al<sub>0.62</sub>Ga<sub>0.38</sub>N doped with a Si concentration of  $3 \times 10^{19} \text{ cm}^{-3}$  was grown on an AlN template [40,41]. Multiple-quantum wells, an Al<sub>0.85</sub>Ga<sub>0.15</sub>N electron blocking layer (EBL), a p-type AlGaIn, and a p<sup>+</sup>-type AlGaIn were grown on the

n-type AlGaIn underlayer. The p<sup>+</sup>-type AlGaIn was doped with Mg at a concentration of  $1.7 \times 10^{20} \text{ cm}^{-3}$ . Subsequently, n<sup>+</sup>-type and n-type AlGaIn were grown under the same conditions as those of the n-type AlGaIn underlayer, as indicated in Figure 1(b). The mesa was formed by dry etching using HCl gas. Thereafter, we formed 20/150/50/100/240-nm-thick V/Al/Ti/Pt/Au electrodes as both n-type AlGaIn electrodes, and they were simultaneously annealed under a nitrogen (N<sub>2</sub>) ambient at 720 °C for 30 s. Further, the annealing process contributes Mg activation under lateral hydrogen diffusion from the exposed mesa-parts of the p-type layers [30,31,68–70]. For comparison, we prepared a conventional pn-diode-based LED with a thin p-type GaN contact layer grown on a p-type AlGaIn shown in Figure 1(a). We adopted indium zinc oxide (IZO) for the anode. The emitted UV light was fully absorbed at the IZO electrode; the sizes of the LED and the anode, and the thickness of the sapphire substrate were 1 mm<sup>2</sup>, 0.56 mm<sup>2</sup>, and 200 μm, respectively. The light output power was measured using an integrating sphere. For the former, we prepared an AlGaIn homoepitaxial TJ LED (TJ#1 to TJ#5) with various Si concentrations and C incorporations in the n<sup>+</sup>-type AlGaIn layer, as summarized in Table 2 [71]. The carbon concentration was approximately  $3.0 \times 10^{18} \text{ cm}^{-3}$  (TJ#1 and TJ#2), and it was reduced to  $6.5 \times 10^{17} \text{ cm}^{-3}$  (TJ#3 to TJ#5) by changing the growth pressure from 50 mbar to 100 mbar. In case of the latter, we prepared MgZnO/Al electrodes for the TJ LED with TJ#5. We deposited a 50-nm-thick MgZnO electrode by RF magnetron sputtering at a substrate temperature of 200 °C, and a typical lift-off process was employed. The sputtering target for MgZnO was prepared as a 2-inch MgZnO sintered material of purity 4N, which is the MgO:ZnO mixing atomic ratio of 1:2. The RF power, sputtering gas, and gas pressure were 100 W, Ar, and approximately  $3.4\text{--}3.5 \times 10^{-1} \text{ Pa}$ , respectively. After forming the MgZnO electrode, the conductivity was improved by annealing at 850 °C for 5 min under N<sub>2</sub> ambient. In the cathode, Ti/Al electrodes were deposited by the electron beam (EB) method and alloyed at 450 °C under N<sub>2</sub> ambient. Al/Ti/Pt/Au electrodes with 300/50/100/240 nm were formed on the MgZnO electrode via the EB method to obtain a high-reflective electrode. The reflectance of the electrodes for TJ LEDs was measured using a UV-visible spectrophotometer (UV-VIS). For comparison, Ti/Al electrodes for the TJ LED anode were prepared via the same process as the cathode.

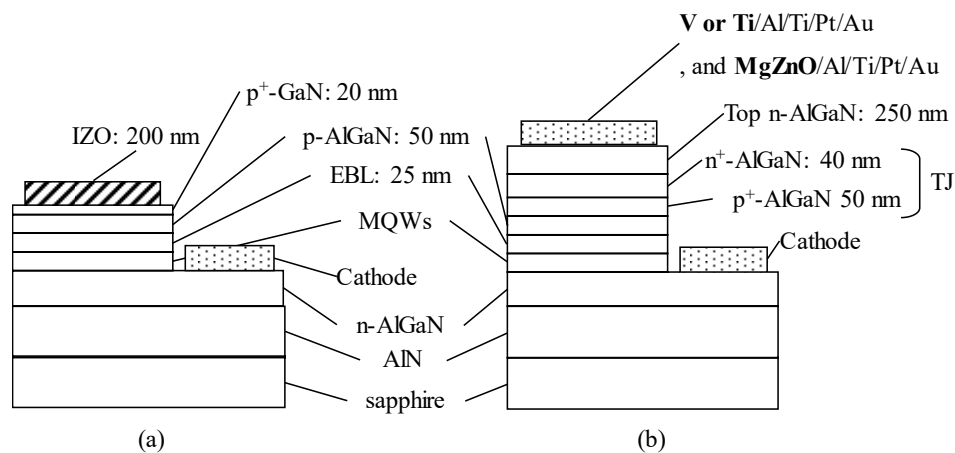


Figure 1. Deep-UV LED structures for (a) PN junction and (b) TJ devices.

**Table 2. Summary of the evaluated parameters for all LEDs.** PN and TJ indicate the PN junction and TJ LEDs, respectively. [Si] and [C] are directly measured for the samples TJ#1, TJ#3, and TJ#4, whereas [Si] and [C] in samples TJ#2 and TJ#5 (labeled by\*) are estimated from the dates for TJ#1, TJ#3, and TJ#4. Copyright 2021 The Japan Society of Applied Physics. [71].

| Sample |    | p-AlGaIn       |     | p <sup>+</sup> -AlGaIn |  | n <sup>+</sup> -AlGaIn   |                         |
|--------|----|----------------|-----|------------------------|--|--------------------------|-------------------------|
|        |    | Al composition |     |                        |  | [Si] (cm <sup>-3</sup> ) | [C] (cm <sup>-3</sup> ) |
| PN     | #1 | 50%            | 50% |                        |  |                          |                         |
|        | #2 | 50%            | 50% |                        |  |                          |                         |

|    |    |     |     |                       |                       |
|----|----|-----|-----|-----------------------|-----------------------|
|    | #1 | 50% | 50% | $6.3 \times 10^{19}$  | $1.8 \times 10^{18}$  |
|    | #2 | 50% | 50% | $1.3 \times 10^{20*}$ | $1.8 \times 10^{18*}$ |
| TJ | #3 | 50% | 50% | $6.3 \times 10^{19}$  | $3.1 \times 10^{17}$  |
|    | #4 | 50% | 50% | $1.3 \times 10^{20}$  | $3.1 \times 10^{17}$  |
|    | #5 | 60% | 60% | $1.3 \times 10^{20*}$ | $3.1 \times 10^{17*}$ |

### 3. Results and Discussions

#### 3.1. AlGa<sub>0.6</sub>N homoepitaxial tunnel-junction deep-UV LEDs with n-type AlGa<sub>0.6</sub>N based on suppressed complex defect formation

Forward voltage–current density characteristics for samples PN#1, TJ#1, TJ#2, TJ#3, and TJ#4 are presented in Figure 2 and measured by direct current (DC) operation at 300 K. The forward voltage (6.6 V) of the conventional PN LED (PN#1) was provided at 63 A/cm<sup>2</sup>. The characteristics were roughly the same as those reported previously [16,72,73]. The forward voltage of the TJ LEDs (TJ#1 and TJ#2) was extremely high and operated at approximately 16 V at 4 A/cm<sup>2</sup>. These TJ LEDs could not perform sufficient current injection; however, a slightly decreasing forward voltage trend was observed for TJ#2 relative to TJ#1. Forward voltages of TJ#3 and TJ#4 were 12.1 V and 10.3 V at 63 A/cm<sup>2</sup>, respectively, and this was significantly reduced by more than 6 V than those of TJ#1 and TJ#2. The high-doping Si concentration of the n<sup>+</sup>-type AlGa<sub>0.6</sub>N was effective in reducing the forward voltage of the AlGa<sub>0.6</sub>N TJ LEDs. Further, suppressing the C incorporation was more effective than the high Si-doping concentration of the n<sup>+</sup>-type AlGa<sub>0.6</sub>N in reducing the forward voltage. The operating voltage of AlGa<sub>0.6</sub>N TJ LEDs could be reduced because the carrier concentration of n<sup>+</sup>-type Al<sub>0.6</sub>Ga<sub>0.4</sub>N was increased by suppressing the C incorporation. The electrical characteristics of the n-type AlGa<sub>0.6</sub>N at 300 K under the van der-Pauw Hall effect were measured. The carrier concentration and resistivity of the n<sup>+</sup>-type Al<sub>0.6</sub>Ga<sub>0.4</sub>N with a Si concentration of  $1.2 \times 10^{20}$  cm<sup>-3</sup> based on TJ#2 was extremely low ( $< 1.0 \times 10^{16}$  cm<sup>-3</sup>) and semi-insulating because of the compensation by C<sub>N</sub>, as shown in Figure 3 (a) and ref. [68]. Those at a Si concentration of  $1.2 \times 10^{20}$  cm<sup>-3</sup> based on TJ#4 were  $3.5 \times 10^{16}$  cm<sup>-3</sup> and 23 Ωcm, respectively, because of the suppression of C incorporation in the n<sup>+</sup>-type AlGa<sub>0.6</sub>N. This improvement contributes to the reduction in the forward voltage for TJ#4 compared to TJ#2.

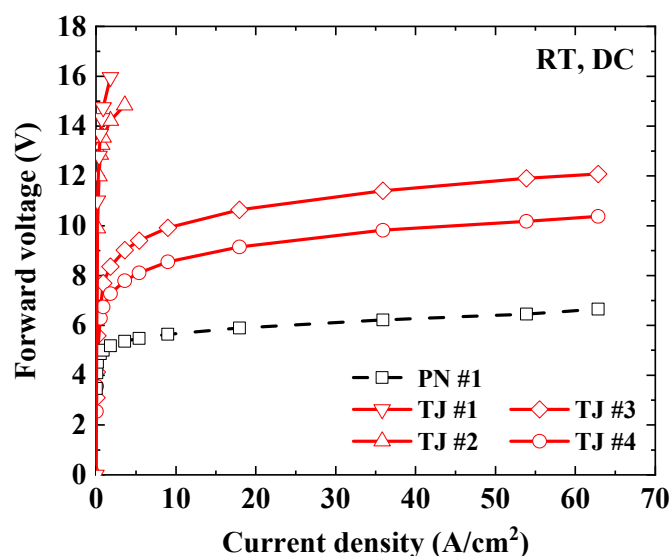


**Figure 2.** Forward voltage–current density characteristics measured by DC operation at room temperature for samples PN#1, TJ#1, TJ#2, TJ#3, and TJ#4. Copyright 2021 The Japan Society of Applied Physics. [68].

The difference in the forward voltages between TJ#3 and TJ#4 suggests that the Si overdose above  $6 \times 10^{19} \text{ cm}^{-3}$  is effective for improving TJ despite the reduction in the carrier concentration with an increase of Si concentration, as shown in Figure 3(b). The reduction of the carrier concentration can be attributed to the self-compensation of  $V_{\text{III}}\text{-nSi}$  complexes [32–41]. However, the depletion layer width was found to be reduced to approximately 10 nm for the Si doping concentration of  $1.2 \times 10^{20} \text{ cm}^{-3}$  [74]. Therefore, the Si overdose can contribute to a reduction in the depletion layer width, which results in an increase in the tunneling probability. Another possibility is trap-assisted tunneling through defects formed by the Si overdose although a further investigation is required. Therefore, we concluded that both the C reduction and high Si doping are keys to reduce the forward voltage of AlGaN-based TJs.

The present TJ structure has very thick TJ layer compared to the depletion layer width of approximately 10 nm shown in Figure 1(b), and it can be a cause of the excess series resistance of the n<sup>+</sup>-type AlGaN layer. We further reduce the operation voltage to 8.8 V at a DC current of 63 A/cm<sup>2</sup> by optimizing the TJ thickness [75].

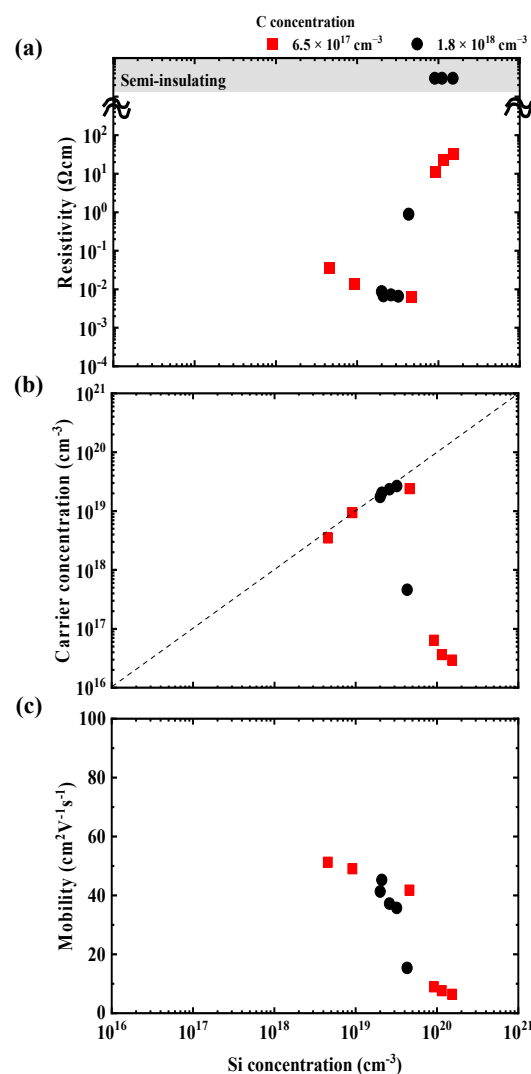


**Figure 3.** Si concentration dependence of (a) resistivity, (b) carrier concentration, and (c) mobility of n-type  $\text{Al}_{0.62}\text{Ga}_{0.38}\text{N}$ . The red square (■) and black circle (●) represent the values of C concentrations of  $1.8 \times 10^{18} \text{ cm}^{-3}$  and  $6.5 \times 10^{17} \text{ cm}^{-3}$ , as grown under pressures 50 mbar and 100 mbar, respectively.

### 3.2. Sputtered polycrystalline MgZnO/Al reflective electrodes for enhanced light emission in AlGaIn-based homoepitaxial tunnel junction DUV-LED

We evaluate MgZnO/Al reflective electrodes for an Al<sub>0.6</sub>Ga<sub>0.4</sub>N TJ LED (TJ#5) to enhance the LEE. The TJ LED of TJ#5 is performed under the optimized growth condition similar to that of TJ#4. These forward voltages are slightly increased by approximately 0.6 V when the Al composition of the p-type AlGaIn increased from 50% (TJ#4) to 60% (TJ#5).

The current density–forward voltage characteristics of the AlGaIn TJ LEDs using conventional Ti/Al and MgZnO electrodes are illustrated in Figure 4(a). The forward voltages of the AlGaIn TJ LEDs using Ti/Al and MgZnO/Al electrodes were 10.8 V and 10.3 V at a DC operation of 63 A/cm<sup>2</sup>, respectively. The forward voltage offset of approximately 1 V was observed for the AlGaIn TJ LED using MgZnO/Al electrodes compared with that using the Ti/Al electrodes at a current density of 30–60 A/cm<sup>2</sup>. In addition, the forward voltages of the TJ LEDs of both Ti/Al and MgZnO/Al electrodes are comparable at a current density above 30 A/cm<sup>2</sup>. Therefore, we realized carrier injection into the TJ LED using MgZnO/Al electrodes. For more details, the contact resistivity and band alignment of the interface between the MgZnO electrode and n-type AlGaIn contact layer are reported in ref. [76].

Figure 4(b) shows the current density–emission power characteristics and emission wavelength spectra of the AlGaIn TJ LEDs. The emission wavelength is 284 nm at a DC operation of 63 A/cm<sup>2</sup>. The output powers of the AlGaIn TJ LEDs with conventional Ti/Al electrodes and MgZnO/Al electrodes are 32.8 and 57.3 mW, respectively, at a DC operation of 63 A/cm<sup>2</sup>. The output power of the TJ LED using MgZnO/Al electrodes is enhanced to approximately 1.7 times using the Ti/Al electrodes. The external quantum efficiencies (EQEs) of the TJ LED using the Ti/Al electrodes and MgZnO/Al electrodes are 2.15% and 3.75%, respectively, at a DC operation of 63 A/cm<sup>2</sup>, as shown in Figure 4(c). The highest output power is realized for AlGaIn TJ LEDs. A maximum EQE of 3.78% is achieved for the AlGaIn TJ LED using MgZnO/Al electrodes. The reflectance at an emission wavelength of 284 nm for the TJ LED with the Ti/Al electrodes and MgZnO/Al electrodes was 9.5% and 20.2%, respectively. The Ti/Al electrodes exhibited low reflectivity because of the alloyed metal. In addition, the MgZnO/Al electrodes exhibited high reflectivity because of the nonalloyed Al separated from the cathode annealing process. Therefore, it contributed to the high reflectance of the TJ LED with MgZnO/Al electrodes.

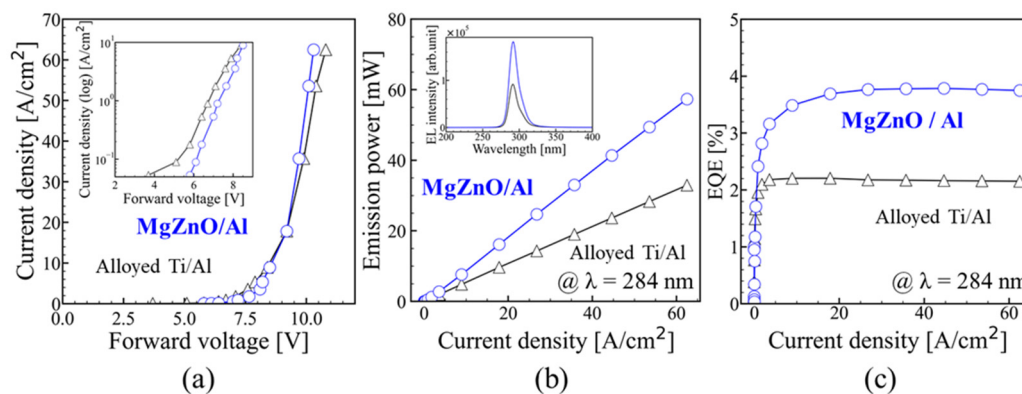


**Figure 4.** (a) Current density–forward voltage, (b) emission power–current density, and (c) EQE–current density characteristics of the fabricated TJ LEDs. Copyright 2022 The Japan Society of Applied Physics [76].

Figure 5(a) shows the absorption coefficient spectrum of only the n-type Al<sub>0.6</sub>Ga<sub>0.4</sub>N template and MgZnO (50 nm) on the n-type Al<sub>0.6</sub>Ga<sub>0.4</sub>N template. The absorption coefficients of both increased near 4.8 eV. The absorption coefficient of MgZnO on the n-type Al<sub>0.6</sub>Ga<sub>0.4</sub>N template increased near 4.0 eV. The band gap of wz-MgZnO is reported to be approximately 3.34–4.0 eV, which depends on the Mg composition [58]. The UV light absorption near 4.0 eV is attributed to wz-MgZnO. Figure 5(b) shows the thickness dependence of the transmittance of MgZnO based on the calculation from its

absorption coefficient  $\alpha = 1.6 \times 10^5 \text{ cm}^{-1}$  at the emission wavelength of 284 nm in the fabricated TJ LED. The transmittance of the MgZnO at a thickness of 50 nm is indicated as approximately 40%. We estimate a transmittance of more than 80% by reducing the MgZnO thickness to less than 10 nm for enhancing the output power of AlGaN LEDs. The TJ LED structure can be optimized by utilizing optical cavity effects toward the improvement of LEE with other enhancement approaches [77,78]. The thickness of the n-type AlGaN in contact with the AlGaN TJ should be optimized in the near future to realize a higher output power.

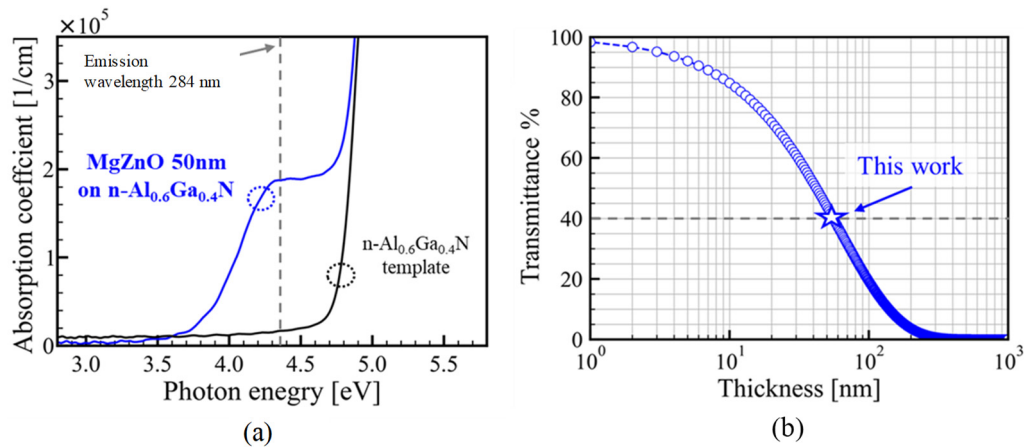


**Figure 5.** Comparison of the absorption coefficient spectra of the n-type Al<sub>0.6</sub>Ga<sub>0.4</sub>N template and MgZnO deposited on the n-type Al<sub>0.6</sub>Ga<sub>0.4</sub>N. (b) Thickness dependence of the transmittance of MgZnO calculated from the absorption coefficient ( $\alpha = 1.6 \times 10^5 \text{ cm}^{-1}$ ) at a photon energy of 4.3 eV. Copyright 2022 The Japan Society of Applied Physics [76].

#### 4. Conclusions

We realized the improvement of the high-Al-composition AlGaN TJ deep-UV LEDs by controlling the growth of n-type AlGaN and polycrystalline MgZnO/Al electrodes. Two essential factors are considered to reduce the operating voltage of AlGaN TJ LEDs by changing the growth condition: suppression of C incorporation and doping of n<sup>+</sup>-type AlGaN at a high Si concentration. The operating voltage of AlGaN TJ LED was 10.8 V at a DC operation of 63 A/cm<sup>2</sup>. Highly reflective MgZnO/Al electrodes were fabricated as anodes for AlGaN TJ LEDs to enhance the output power of the AlGaN TJ LEDs. The output power of the 57.3 mW of TJ LED using MgZnO/Al electrodes was realized at an emission wavelength of 284 nm under the DC operation of 63 A/cm<sup>2</sup>; this was 1.7 times higher than that when using a conventional Ti/Al electrode. In the near future, the output power can be further improved by lessening the thickness of the MgZnO for AlGaN TJ LEDs.

**Author Contributions:** K. Nagata and T. Matsubara: writing – original draft preparation, K. Nagata, Y. Saito, M. Kushimoto, S. Tomai, S. Katsumata, Y. Honda, T. Takeuchi, and H. Amano; writing-review and editing, supervision, H. Amano. All authors have read and agreed to the published version of the manuscript.

**Informed Consent Statement:** Not applicable.

**Acknowledgments:** This work was supported by the MOE Program for the implementation of the innovative infection control and digital technologies with low CO<sub>2</sub> emission.

**Conflicts of Interest:** The authors declare no conflict of interest.

## References

1. Oguma, K.; Rattanakul, S. UV inactivation of viruses in water: its potential to mitigate current and future threats of viral infectious diseases. *Jpn. J. Appl. Phys.* **2021**, *60*, 110502.
2. Minamikawa, T.; Koma, T.; Suzuki, A.; Nagamatsu, K.; Yasui, T.; Yasutomo, K.; Nomaguchi, M. Inactivation of SARS-CoV-2 by deep ultraviolet light emitting diode: A review. *Jpn. J. Appl. Phys.* **2021**, *60*, 090501.
3. Muramoto, Y.; Kimura, M.; Kondo, A. Verification of inactivation effect of deep-ultraviolet LEDs on bacteria and viruses, and consideration of effective irradiation methods. *Jpn. J. Appl. Phys.* **2021**, *60*, 090601.
4. Inagaki, H.; Saito, A.; Sugiyama, H.; Okabayashi, T.; Fujimoto, S. Rapid inactivation of SARS-CoV-2 with deep-UV LED irradiation. *Emerging Microbes Infect.* **2020**, *9*, 1744.
5. Saito, Y.; Wada, S.; Nagata, K.; Makino, H.; Boyama, S.; Miwa, H.; Matsui, S.; Kataoka, K.; Narita, T.; Horibuchi, K. Efficiency improvement of AlGaIn-based deep-ultraviolet light-emitting diodes and their virus inactivation application. *Jpn. J. Appl. Phys.* **2021**, *60*, 080501.
6. Amano, H.; Collazo, R.; Santi, C. D.; Einfeldt, S.; Funato, M.; Glaab, J.; Hagedorn, S.; Hirano, A.; Hirayama, H.; Ishii, R.; Kashima, Y.; Kawakami, Y.; Kirste, R.; Kneissl, M.; Martin, R.; Mehnke, F.; Meneghini, M.; Ougazzaden, A.; J Parbrook, P.; Rajan, S.; Reddy, P.; Römer, F.; Rusche, J.; Sarkar, B.; Scholz, F.; J Schowalter, L. Shields, P.; Sitar, Z.; Sulmoni, L.; Wang, T.; Wernicke, T.; Weyers, M.; Witzigmann, B.; Wu, Y.; Wunderer, T.; and Zhang, Y.; The 2020 UV emitter roadmap. *J. Phys. D: Appl. Phys.* **2020**, *53*, 503001.
7. Ichikawa, M.; Endo, S.; Sagawa, H.; Fujioka, A.; Kosugi, T.; Mukai, T.; Uomoto, M.; Shimatsu, T. High-output-power deep ultraviolet light-emitting diode assembly using direct bonding. *ECS Trans.* **2016**, *75*, 53.
8. Muth, J. F.; Brown, J. D.; Johnson, M. A. L.; Yu, Z.; Kolbas, R. M.; Cook, Jr J. W.; Schetzina, J. F. Absorption coefficient and refractive index of GaN, AlN and AlGaIn alloys. *MRS Internet J. Nitride Semicond. Res.* **1999**, *4S1*, G5.2.
9. Katsuragawa, M.; Sota, S.; Komori, M.; Anbe, C.; Takeuchi, T.; Sakai, H.; Amano, H.; Akasaki, I. Thermal ionization energy of Si and Mg in AlGaIn. *J. Cryst. Growth* **1998**, *189/190*, 528.
10. Jeon, S. R.; Ren, Z.; Cui, G.; Su, J.; Gherasimova, M.; Han, J.; Cho, H. K.; Zhou, L. Investigation of Mg doping in high-Al content p-type Al<sub>x</sub>Ga<sub>1-x</sub>N. *Appl. Phys. Lett.* **2005**, *86*, 082107.
11. Nakarmi, M. L.; Kim, K. H.; Khizar, M.; Fan, Z. Y.; Lin, J. Y.; Jiang, H. X. Electrical and optical properties of Mg-doped Al<sub>0.7</sub>Ga<sub>0.3</sub>N alloys. *Appl. Phys. Lett.* **2005**, *86*, 092108.
12. Nakarmi, M. L.; Nepal, N.; Ugolini, C.; Altahtamouni, T. M.; Lin, J. Y.; Jiang, H. X. Correlation between optical and electrical properties of Mg-doped AlN epilayers. *Appl. Phys. Lett.* **2006**, *89*, 152120.
13. Szabó, Á.; Son, N. T.; Janzén, E.; Gali, A. Stampfl, C.; Neugebauer, J.; Group-II acceptors in wurtzite AlN: A screened hybrid density functional study. *Appl. Phys. Lett.* **2010**, *96*, 192110.
14. Lyons, J. L.; Janotti, A.; Van de Walle, C. G. Shallow versus Deep Nature of Mg Acceptors in Nitride Semiconductors. *Phys. Rev. Lett.* **2012**, *108*, 156403.
15. Takano, T.; Mino, T.; Sakai, J.; Noguchi, N.; Tsubaki, K.; Hirayama, H. Deep-ultraviolet light-emitting diodes with external quantum efficiency higher than 20% at 275 nm achieved by improving light-extraction efficiency. *Appl. Phys. Exp.* **2017**, *10*, 03100.
16. Lee, S.Y.; Han, D.S.; Lee, Y.G.; Choi, K.K.; Oh, J.T.; Jeong, H.H.; Seong, T.Y.; Amano, H. Heavy Mg doping to form reliable Rh reflective ohmic contact for 278 nm deep ultraviolet AlGaIn-based light-emitting diodes. *ECS J. Solid State Sci. Technol.* **2020**, *9*, 065016.
17. France, R.; Xu, T.; Chen, P.; Chandrasekaran, R.; Moustakas, T. Vanadium-based Ohmic contacts to n-AlGaIn in the entire alloy composition. *Appl. Phys. Lett.* **2007**, *90*, 062115.
18. Mori, K.; Takeda, K.; Kusafuka, T.; Iwaya, M.; Takeuchi, T.; Kamiyama, S.; Akasaki, I.; Amano, H. Low-ohmic-contact-resistance V-based electrode for n-type AlGaIn with high AlN molar fraction. *Jpn. J. Appl. Phys.* **2016**, *55*, 05FL03.
19. Nagata, N.; Senga, T.; Iwaya, M.; Takeuchi, T.; Kamiyama, S.; Akasaki, I. Reduction of contact resistance in V-based electrode for high AlN molar fraction n-type AlGaIn by using thin SiNx intermediate layer. *Phys. Status Solidi c* **2016**, *14*, 1600243.
20. Krishnamoorthy, S.; Akyol, F.; Park, P.S.; Rajan, S. Low resistance GaN/InGaIn/GaN tunnel junctions. *Appl. Phys. Lett.* **2013**, *102*, 113503.
21. Minamikawa, D.; Ino, M.; Kawai, S.; Takeuchi, T.; Kamiyama, S.; Iwaya, M.; Akasaki, I. GaInN-based tunnel junctions with high InN mole fractions grown by MOVPE. *Phys. Status Solidi B* **2014**, *252*, 1127.

22. Yonkee, B.P.; Young, E.C.; Lee, C.; Leonard, J.T.; DenBaars, S.P.; Speck, J.S.; Nakamura, S. Demonstration of a III-nitride edge-emitting laser diode utilizing a GaN tunnel junction contact. *Opt. Express* **2016**, *24*, 7816.
23. Neugebauer, S.; Hoffmann, M.P.; Witte, H.; Bläsing, J.; Dadgar, A.; Strittmatter, A.; Niermann, T.; Narodovitch, M.; Lehmann, M. All metalorganic chemical vapor phase epitaxy of p/n-GaN tunnel junction for blue light emitting diode applications. *Appl. Phys. Lett.* **2017**, *110*, 102104.
24. Hwang, D.; Mughal, A.J.; Wong, M.S.; Alhassan, A.I.; Nakamura, S.; DenBaars, S.P. Micro-light-emitting diodes with III-nitride tunnel junction contacts grown by metalorganic chemical vapor deposition. *Appl. Phys. Exp.* **2018**, *11*, 012102.
25. Akatsuka, Y.; Iwayama, S.; Takeuchi, T.; Kamiyama, S.; Iwaya, M.; Akasaki, I. Doping profiles in low resistive GaN tunnel junctions grown by metalorganic vapor phase epitaxy. *Appl. Phys. Exp.* **2019**, *12*, 025502.
26. Zhang, Y.; Krishnamoorthy, Y.; Akyol, F.; Allerman, A.A.; Moseley, M.W.; Armstrong, A.M.; Rajan, S. Design and demonstration of ultra-wide bandgap AlGaIn tunnel junctions. *Appl. Phys. Lett.* **2016**, *109*, 121102.
27. Zhang, Y.; Krishnamoorthy, S.; Akyol, F.; Bajaj, S.; Allerman, A.A.; Moseley, M.W.; Armstrong, A.M.; Rajan, S. Tunnel-injected sub-260 nm ultraviolet light emitting diodes. *Appl. Phys. Lett.* **2017**, *110*, 201102.
28. Zhang, Y.; Jamal-Eddine, Z.; Akyol, F.; Bajaj, S.; Johnson, J.M.; Calderon, G.; Allerman, A.A.; Moseley, M.W.; Armstrong, A.M.; Hwang, J.; Rajan, S. Tunnel-injected sub 290 nm ultra-violet light emitting diodes with 2.8% external quantum efficiency. *Appl. Phys. Lett.* **2018**, *112*, 071107.
29. Pandey, A.; Shin, W.J.; Gim, J.; Hovden, R.; Mi, Z. High-efficiency AlGaIn/GaN/AlGaIn tunnel junction ultraviolet light-emitting diodes. *Photon. Res.* **2020**, *8*, 331.
30. Fan Arcara, V.; Damilano, B.; Feuillet, G.; Vézian, S.; Ayadi, K.; Chenot, S.; Duboz, J.Y. Ge doped GaN and Al<sub>0.5</sub>Ga<sub>0.5</sub>N-based tunnel junctions on top of visible and UV light emitting diodes. *J. Appl. Phys.* **2019**, *126*, 224503.
31. Kuhn, C.; Sulmoni, L.; Guttman, M.; Glaab, J.; Susilo, N.; Wernicke, T.; Weyers, M.; Kneissl, M. MOVPE-grown AlGaIn-based tunnel heterojunctions enabling fully transparent UVC LEDs. *Photon. Res.* **2019**, *7*, B7.
32. Nakamura S.; Mukai, T.; Senoh, M.; Iwasa, N. Thermal annealing effects on P-type Mg-doped GaN Films. *Jpn. J. Appl. Phys.* **1992**, *31*, L139.
33. Nakamura, S.; Iwasa, N.; Senoh, M.S.; Mukai, T. Hole compensation mechanism of P-type GaN Films. *Jpn. J. Appl. Phys.* **1992**, *31*, 1258.
34. Limpijumnong, S.; Northrup, J.E.; Van de Walle, C.G. Identification of hydrogen configurations in p-type GaN through first-principles calculations of vibrational frequencies, *Phys. Rev. B*, **2003**, *68*, 075206.
35. Narita, T.; Yoshida, H.; Tomita, K.; Kataoka, K.; Sakurai, H.; Horita, M.; Bockowski, M.; Ikarashi, N.; Suda, J.; Kachi, T.; Tokuda, Y. Progress on and challenges of p-type formation for GaN power devices. *J. Appl. Phys.* **2020**, *128*, 090901.
36. Nam, K. B.; Nakarmi, M. L.; Lin, J. Y.; Jiang, H. X. Photoluminescence studies of Si-doped AlN epilayers. *Appl. Phys. Lett.* **2005**, *86*, 222108.
37. Nepal, N.; Nakarmi, M. L.; Lin, J. Y.; Jiang, H. X. Photoluminescence studies of impurity transitions in AlGaIn alloys. *Appl. Phys. Lett.* **2006**, *89*, 092107.
38. Chichibu, S. F.; Miyake, H.; Ishikawa, Y.; Tashiro, M.; Ohtomo, T.; Furusawa, K.; Hazu, K.; Hiramatsu, K.; Uedono, A. The origins and properties of intrinsic nonradiative recombination centers in wide bandgap GaN and AlGaIn. *J. Appl. Phys.* **2013**, *113*, 213506.
39. Bryan, I.; Bryan, Z.; Washiyama, S.; Reddy, P.; Gaddy, B.; Sarkar, B.; Breckenridge, M. H.; Guo, Q.; Bobea, M.; Tweedie, J.; Mita, S.; Irving, D.; Collazo, R.; Sitar, Z. The role of transient surface morphology on composition control in AlGaIn layers and wells. *Appl. Phys. Lett.* **2018**, *112*, 062102.
40. Nagata, K.; Makino, H.; Yamamoto, T.; Kataoka, K.; Narita, T.; Saito, Y. Low resistivity of highly Si-doped n-type Al<sub>0.62</sub>Ga<sub>0.38</sub>N layer by suppressing self-compensation. *Appl. Phys. Exp.* **2020**, *13*, 025504.
41. Kataoka, K.; Narita, T.; Nagata, K.; Makino, H.; Saito, Y. Electronic degeneracy conduction in highly Si-doped Al<sub>0.6</sub>Ga<sub>0.4</sub>N layers based on the carrier compensation effect. *Appl. Phys. Lett.* **2020**, *117*, 262103.
42. Piao, G.; Ikenaga, K.; Yano, Y.; Tokunaga, H.; Mishima, A.; Ban, Y.; Tabuchi, T.; Matsumoto, K. Study of carbon concentration in GaN grown by metalorganic chemical vapor deposition. *J. Cryst. Growth* **2016**, *456*, 137.

43. Sawada, N.; Narita, T.; Kanechika, M.; Uesugi, T.; Kachi, T.; Horita, M.; Kimoto, T.; Suda, J. Sources of carrier compensation in metalorganic vapor phase epitaxy-grown homoepitaxial n-type GaN layers with various doping concentrations. *Appl. Phys. Exp.* **2018**, *11*, 041001.
44. Kanegae, K.; Fujikura, H.; Otoki, Y.; Konno, T.; Yoshida, T.; Horita, M.; Kimoto, T.; Suda, J. Deep-level transient spectroscopy studies of electron and hole traps in n-type GaN homoepitaxial layers grown by quartz-free hydride-vapor-phase epitaxy. *Appl. Phys. Lett.* **2019**, *115*, 012103.
45. Narita, T.; Tomita, K.; Kataoka, K.; Tokuda, Y.; Kogiso, T.; Yoshida, H.; Ikarashi, N.; Iwata, K.; Nagao, M.; Sawada, N.; Horita, M.; Suda, J.; Kachi, T. Overview of carrier compensation in GaN layers grown by MOVPE: toward the application of vertical power devices. *Jpn. J. Appl. Phys.* **2020**, *59*, SA0804.
46. Lyons, J.L.; Janotti, A.; Van de Walle, C.G. Effects of carbon on the electrical and optical properties of InN, GaN, and AlN. *Phys. Rev. Lett.* **2014**, *89*, 035204.
47. Nagasawa, Y.; Hirano, A. A review of AlGaN-based deep-ultraviolet light-emitting diodes on sapphire. *Appl. Sci.* **2018**, *8*, 1264.
48. Ichikawa, M.; Fujioka, A.; Kosugi, T.; Endo, S.; Sagawa, H.; Tamaki, H.; Mukai, T.; Uomoto, M.; Shimatsu, T. High-output-power deep ultraviolet light-emitting diode assembly using direct bonding. *Appl. Phys. Exp.* **2016**, *9*, 072101.
49. Zhou, S.; Liu, X.; Gao, Y.; Liu, Y.; Liu, M.; Liu, Z.; Gui, C.; Liu, S. Numerical and experimental investigation of GaN-based flip-chip light-emitting diodes with highly reflective Ag/TiW and ITO/DBR Ohmic contacts. *Opt. Exp.* **2017**, *25*, 26615.
50. Zhou, S.; Zheng, C.; Lv, J.; Gao, Y.; Wang, R.; Liu, S. GaN-based flip-chip LEDs with highly reflective ITO/DBR p-type and via hole-based n-type contacts for enhanced current spreading and light extraction. *Opt. Laser Technol.* **2017**, *92*, 95.
51. Mizuhashi, M. Electrical properties of vacuum-deposited indium oxide and indium tin oxide films. *Thin Solid Films*, **1980**, *70*, 91.
52. Liu, J.; Wu, D.; Zeng, S. Influence of temperature and layers on the characterization of ITO films. *J. Mater. Process Technol.* **2009**, *209*, 3943.
53. Singh, A.; Chaudhary, S.; Pandya, D.K. High conductivity indium doped ZnO films by metal target reactive co-sputtering. *Acta Materialia* **2016**, *111*, 1.
54. Cao, Y.; Miao, L.; Tanemura, S.; Tanemura, M.; Kuno, Y.; Hayashi, Y.; Mori, Y. Optical properties of indium-doped ZnO films. *Jpn. J. Appl. Phys.* **2006**, *45*, 1623.
55. Kumar, P.M.R.; Kartha, C.S.; Vijayakumar, K.P.; Abe, T.; Kashiwaba, Y.; Singh, F.; Avasthi, D.K. On the properties of indium doped ZnO thin films. *Semicond. Sci. Technol.* **2005**, *20*, 120.
56. Rahmane, S.; Djouadi, M.A.; Aida, M.S.; Barreau, N.; Abdallah, B.; Hadj Zoubir, N. Power and pressure effects upon magnetron sputtered aluminum doped ZnO films properties. *Thin Solid Films* **2010**, *519*, 5.
57. Jiménez-González, A.E.; Urueta, J.A.S.; Suárez-Parra, R. Optical and electrical characteristics of aluminum-doped ZnO thin films prepared by solgel technique. *J. Cryst. Growth* **1998**, *192*, 430.
58. Minami, T.; Miyata, T.; Yamamoto, T.; Toda, H. Origin of electrical property distribution on the surface of ZnO:Al films prepared by magnetron sputtering. *J. Vac. Sci. Technol. A* **2000**, *18*, 1584.
59. Choi, B.H.; Im, H.B.; Song, J.S.; Yoon, K.H. Optical and electrical properties of Ga<sub>2</sub>O<sub>3</sub>-doped ZnO films prepared by r.f. sputtering. *Thin Solid Films* **1990**, *193-194*, 712.
60. Song, P.K.; Watanabe, M.; Kon, M.; Mitsui, A.; Shigesato, Y. Electrical and optical properties of gallium-doped zinc oxide films deposited by dc magnetron sputtering. *Thin Solid Films* **2002**, *411*, 82.
61. Wang, X.; Saito, K.; Tanaka, T.; Nishio, M.; Nagaoka, T.; Arita, M.; Guo, Q. Energy band bowing parameter in MgZnO alloys. *Appl. Phys. Lett.* **2015**, *107*, 022111.
62. Wang, X.; Saito, K.; Tanaka, T.; Nishio, M.; Guo, Q. Lower temperature growth of single phase MgZnO films in all Mg content range. *J. Alloys Compd.* **2015**, *627*, 383.
63. Kushimoto, M.; Sakai, T.; Ueoka, Y.; Tomai, S.; Katsumata, S.; Deki, M.; Honda, Y.; Amano, H. Effect of annealing on the electrical and optical properties of MgZnO films deposited by radio frequency magnetron sputtering. *Phys. Status Solidi A* **2020**, *217*, 1900955.
64. Borysiewicz, M.A.; Wzorek, M.; Gołaszewska, K.; Kruszka, R.; Pagowska, K.D.; Kamińska, E. Nanocrystalline sputter-deposited ZnMgO:Al transparent p-type electrode in GaN-based 385 nm UV LED for significant emission enhancement. *Materials Science and Engineering: B* **2015**, *200*, 93.
65. Borysiewicz, M.A. ZnO as a functional material, a review. *Crystals* **2019**, *9*, 505.

66. Imura, M.; Nakano, K.; Fujimoto, N.; Okada, N.; Balakrishnan, K.; Iwaya, M.; Kamiyama, S.; Amano, H.; Akasaki, I.; Noro, T.; Takagi, T.; Bandoh, A. Dislocations in AlN Epilayers Grown on Sapphire Substrate by High-Temperature Metal-Organic Vapor Phase Epitaxy. *Jpn. J. Appl. Phys.* **2007**, *46*, 1458.
67. Nagata, K.; Makino, H.; Yamamoto, T.; Saito, Y.; Miki, H. Origin of optical absorption in AlN with air voids. *Jpn. J. Appl. Phys.* **2019**, *58*, SCCC29.
68. Kuwano, Y.; Kaga, M.; Morita, T.; Yamashita, K.; Yagi, K.; Iwaya, M.; Takeuchi, T.; Kamiyama, S.; Akasaki, I. Lateral hydrogen diffusion at p-GaN layers in nitride-based light emitting diodes with tunnel junctions. *Jpn. J. Appl. Phys.* **2013**, *52*, 08JK12.
69. Alhassan, A. I.; Young, E. C.; Alyamani, A. Y.; Albadri, A.; Nakamura, S.; DenBaars, S. P.; Speck, J. S. Reduced-droop green III-nitride light-emitting diodes utilizing GaN tunnel junction. *Appl. Phys. Exp.* **2018**, *11*, 042101.
70. Narita, T.; Tomita, K.; Yamada, S.; Kachi, T. Quantitative investigation of the lateral diffusion of hydrogen in p-type GaN layers having NPN structures. *Appl. Phys. Exp.* **2019**, *12*, 011006.
71. Nagata, K.; Makino, H.; Miwa, H.; Matsui, S.; Boyama, S.; Saito, Y.; Kushimoto, M.; Honda, Y.; Takeuchi, T.; Amano, H. Reduction in operating voltage of AlGaIn homojunction tunnel junction deep-UV light-emitting diodes by controlling impurity concentrations. *Appl. Phys. Exp.* **2021**, *14*, 084001.
72. Inazu, T.; Fukahori, S.; Pernot, C.; Kim, M. H.; Fujita, T.; Nagasawa, Y.; Hirano, A.; Ippommatsu, M.; Iwaya, M.; Takeuchi, T.; Kamiyama, S.; Yamaguchi, M. Honda, Y.; Amano, H.; Akasaki, I. Improvement of light extraction efficiency for AlGaIn-based deep ultraviolet light-emitting diodes. *Jpn. J. Appl. Phys.* **2011**, *50*, 122101.
73. Sung, Y. J.; Kim, M.; Kim, H.; Choi, S.; Kim, Y. H.; Jung, M.; Choi, R.; Moon, Y.; Oh, J.; Jeong, H.; Yeom, G. Y. Light extraction enhancement of AlGaIn-based vertical type deep-ultraviolet light-emitting-diodes by using highly reflective ITO/Al electrode and surface roughening. *Opt. Exp.* **2019**, *27*, 29930.
74. Nagata, K.; Anada, S.; Saito, Y.; Kushimoto, M.; Honda, Y.; Takeuchi, T.; Yamamoto, K.; Hirayama, T.; Amano, H. Visualization of depletion layer in AlGaIn homojunction p-n junction. *Appl. Phys. Exp.* **2022**, *15*, 036504.
75. Nagata, K.; Anada, S.; Miwa, H.; Matsui, S.; Boyama, S.; Saito, Y.; Kushimoto, M.; Honda, Y.; Takeuchi, T.; Amano, H. Structural design optimization of 279 nm wavelength AlGaIn homojunction tunnel junction deep-UV light-emitting diode. *Appl. Phys. Exp.* **2022**, *15*, 044003.
76. Matsubara, T.; Nagata, K.; Kushimoto, M.; Tomai, S.; Katsumata, S.; Honda, Y.; Amano, H. Sputtered polycrystalline MgZnO/Al reflective electrodes for enhanced light emission in AlGaIn-based homojunction tunnel junction DUV-LED. *Appl. Phys. Exp.* **2022**, *15*, 044001.
77. Shen, Y. C.; Wierer, J. J.; Krames, M. R.; Ludowise, M. J.; Misra, M. S.; Ahmed, F. Kim, A. Y.; Mueller, G. O.; Bhat, J. C.; Stockman, S. A.; Martin, P. S. Optical cavity effects in InGaIn/GaN quantum-well-heterostructure flip-chip light-emitting diodes. *Appl. Phys. Lett.* **2003**, *82*, 2221.
78. Matsukura, Y.; Inazu, T.; Pernot, C.; Shibata, N.; Kushimoto, M.; Deki, M.; Honda, Y.; Amano, H. Improving light output power of AlGaIn-based deep-ultraviolet light-emitting diodes by optimizing the optical thickness of p-layers. *Appl. Phys. Exp.* **2021**, *14*, 084004.

**Disclaimer/Publisher's Note:** The statements, opinions and data contained in all publications are solely those of the individual author(s) and contributor(s) and not of MDPI and/or the editor(s). MDPI and/or the editor(s) disclaim responsibility for any injury to people or property resulting from any ideas, methods, instructions or products referred to in the content.